Published in final edited form as:
Neuroimage. 2011 February 14; 54(4): 2623–2634. doi:10.1016/j.neuroimage.2010.11.023.

Beneficial network effects of methylene blue in an amnestic model

Penny D. Riha[a], **Julio C. Rojas**[a], and **F. Gonzalez-Lima**[a,*]
[a] Departments of Psychology, Pharmacology and Toxicology, University of Texas at Austin

Abstract

Posterior cingulate/retrosplenial cortex (PCC) hypometabolism is a common feature in amnestic mild cognitive impairment and Alzheimer's disease. In rats, PCC hypometabolism induced by mitochondrial dysfunction induces oxidative damage, neurodegeneration and memory deficits. USP methylene blue (MB) is a diaminophenothiazine drug with antioxidant and metabolic-enhancing properties. In rats, MB facilitates memory and prevents neurodegeneration induced by mitochondrial dysfunction. This study tested the memory-enhancing properties of systemic MB in rats that received an infusion of sodium azide, a cytochrome oxidase inhibitor, directly into the PCC. Lesion volumes were estimated with unbiased stereology. MB's network-level mechanism of action was analyzed using graph theory and structural equation modeling based on cytochrome oxidase histochemistry-derived metabolic mapping data. Sodium azide infusions induced PCC hypometabolism and impaired visuospatial memory in a holeboard food-search task. Isolated PCC cytochrome oxidase inhibition disrupted the cingulo-thalamo-hippocampal effective connectivity, decreased the PCC functional networks and created functional redundancy within the thalamus. An intraperitoneal dose of 4 mg/kg MB prevented the memory impairment, reduced the PCC metabolic lesion volume and partially restored the cingulo-thalamo-hippocampal network effects. The effects of MB were dependent upon the local sub-network necessary for memory retrieval. The data support that MB's metabolic-enhancing effects are contingent upon the neural context, and that MB is able to boost coherent and orchestrated adaptations in response to physical alterations to the network involved in visuospatial memory. These results implicate MB as a candidate intervention to improve memory. Because of its neuroprotective properties, MB may have disease-modifying effects in amnestic conditions associated with hypometabolism.

Keywords

mild cognitive impairment; memory-enhancement; mitochondrial dysfunction; neuroprotection; graph theory; structural equation modeling

1. INTRODUCTION

Lesions of the posterior cingulate/retrosplenial cortex (PCC) in animals and humans produce amnesia (Riha et al., 2008; Valenstein et al., 1987). Importantly, the PCC is the brain region

*Corresponding author: Prof. Dr. F. Gonzalez-Lima, University of Texas at Austin, 1 University Station A8000, Austin, TX 78712, Tel.: 512-471-5895; Fax: 512-471-4728, gonzalez-lima@mail.utexas.edu.

Conflict of interest. There is no conflict of interest.

with the earliest metabolic decrease in patients at risk of developing Alzheimer's disease (AD) (Minoshima et al., 1997) as well as in transgenic mouse models of AD (Reiman et al., 2000; Valla et al., 2006). PCC hypometabolism is also a common finding in asymptomatic individuals with familial AD and in patients with amnestic mild cognitive impairment (aMCI) who later develop sporadic AD (Chetelat et al., 2003; Drzezga et al., 2003; Mosconi, 2005; Mosconi et al., 2008; Pagani et al., 2009). PCC hypometabolism correlates with the development of temporal lobe atrophy in patients with AD (Mosconi et al., 2006) and is a better predictor of early decline in cognitive function than cerebrospinal fluid levels of β-amyloid and tau proteins (Jagust et al., 2009). In addition to showing the earliest decrease in energy metabolism in patients at risk of AD, the PCC is a major component of the limbic circuit implicated in visuospatial memory. Neuropsychological testing shows that visuospatial abilities are the first to be affected in patients with aMCI (Johnson et al., 2009), and numerous animal and human studies support that PCC dysfunction leads to visuospatial memory impairment (Bussey et al., 1996; Vann and Aggleton, 2002; Whishaw et al., 2001).

Regional hypometabolism in patients at risk for AD is related to mitochondrial dysfunction (Gonzalez-Lima et al., 1998; Mosconi et al., 2009). The brains of postmortem AD patients have local decreases in the mitochondrial enzyme cytochrome oxidase in the PCC (Valla et al., 2001). Cytochrome oxidase is the terminal enzyme of the respiratory chain and its expression is tightly coupled to neuronal oxidative energy demands. Cytochrome oxidase is the rate limiting enzyme for adenosine triphosphate (ATP) synthesis and its activity constitutes a reliable endogenous biomarker of neuronal oxidative energy metabolism (Wong-Riley, 1989). Experimental inhibition of brain cytochrome oxidase activity causes memory deficits in spatial tests such as the Morris water maze, radial arm maze, and holeboard task (Bennett et al., 1992; Bennett and Rose, 1992; Callaway et al., 2004). Recently, we showed that sodium azide, a specific cytochrome oxidase inhibitor, infused directly into the PCC of the rat successfully modeled the visuospatial memory deficits and PCC hypometabolism implicated in aMCI (Riha et al., 2008). The purpose of this model was not to produce large memory deficits; but rather to induce reliable yet small memory impairment comparable to the mild amnestic symptoms found in aMCI. These metabolic and behavioral effects were mediated by decreases in oxygen consumption and ATP production, and increases in oxidative stress (Riha et al., 2008; Swerdlow et al., 1997).

The present study used this novel animal model of PCC cytochrome oxidase inhibition induced by sodium azide local infusion to test the neuroprotective and memory-enhancing effects of pharmaceutical grade (USP) methylene blue (MB). MB is an autoxidizable redox drug that enhances electron flow in the mitochondrial respiratory chain and displays potent antioxidant properties (Scott and Hunter, 1966; Wainwright and Crossley, 2002). Due to its redox potential which is intermediate between that of endogenous electron donors (e.g., NADH, $FADH_2$) and oxygen, MB mimics the activity of coenzyme Q as an electron shuttle in the respiratory chain (Bruchey and Gonzalez-Lima, 2008; Scott and Hunter, 1966). Low-dose MB enhances brain cytochrome oxidase activity after *in vivo* administration to rats (Callaway et al., 2004; Gonzalez-Lima and Bruchey, 2004) and low-dose MB enhances memory in normal rats when given during memory consolidation (Martinez Jr. et al., 1978). MB has also been effective at preventing the spatial memory deficits induced by chronic systemic sodium azide administration in rats (Callaway et al., 2002). In addition, MB displays potent neuroprotective effects when locally co-infused with mitochondrial toxins in the retina and the striatum (Furian et al., 2007; Rojas et al., 2009a; 2009b; Zhang et al., 2006) but its functional effects against localized PCC hypometabolism at the behavioral and brain systems levels have not yet been studied. A holeboard food-search task was used to examine visuospatial abilities of rats to recall the pattern of distribution of appetitive stimuli. We hypothesized that systemic MB will prevent the memory deficits induced by the local

infusion of sodium azide into the PCC by influencing brain circuits mediating visuospatial memory.

2. METHODS

2.1 Subjects

Thirty adult male Sprague Dawley rats (219–255 g) (Harlan, Houston, TX) were single-housed on a 12 h light-dark schedule and allowed to drink water *ad libitum*. For motivational purposes, rats were habituated to sucrose pellets and placed on a food restriction protocol that ensured they did not weigh less than 85% of free-feeding rats of a similar age. All procedures followed NIH guidelines and were approved by the Institutional Animal Care and Use Committee.

2.2 Behavioral procedures

2.2.1 Visuospatial reference memory—Visuospatial reference memory was tested using a holeboard apparatus described previously (Riha et al., 2008). Following habituation, rats were trained to learn a spatial pattern of baited holes. Four holes were baited in a consistent pattern for all subjects throughout training. A trial started as soon as the first hole was nosepoked and ended immediately after the last bait was consumed, or after 5 minutes elapsed. The rats received 5 trials per day for at least 8 days. Training was stopped when 60% reference memory was attained or for a maximum of 14 training days. Rats were matched into treatment groups based on their averaged reference memory scores across all days of training. Reference memory was calculated as the ratio of visits to baited holes divided by the number of visits to all holes. Surgery was performed the day after each rat's last training trial. Following a 24 h recovery period, subjects received an unbaited probe trial to test for memory retention.

2.2.2 Locomotor activity—Locomotor activity was assessed in an open field chamber (MED Associates, St. Albans, VT) to examine the nonspecific effects of the experimental manipulations. One 5 min trial was conducted on training days 5–7 and second one was done following the unbaited probe trial.

2.2.3 Surgery and treatments—Infusions of sodium azide into the PCC were done following the procedure described by Riha et al (2008). The rats in the azide (AZ) and azide plus MB (AZ+MB) groups received 3 M sodium azide in phosphate buffer (pH 7.4). Four bilateral infusions (0.05 μL/min over 10 min), two in each hemisphere, were made at stereotaxic coordinates (in mm): A/P −2.8 and −3.3; M/L ±0.2 to 0.4; D/V −1.2 to −1.3, corresponding to the PCC (i.e., retrosplenial cortex of the rat brain). Subjects in the AZ+MB group (n=9) were injected intraperitoneally with 4 mg/kg USP grade MB (Faulding Pharmaceuticals, Paramus, NJ) immediately after surgery. Subjects in the sham-operated control (n=10) and AZ (n=10) groups received an equivalent volume of 0.9% saline intraperitoneally.

2.3 Brain analyses

2.3.1 Brain processing & cytochrome oxidase histochemistry—After the second assessment of locomotor activity (24 hrs after surgery), the rats were killed by decapitation. Their brains were quickly extracted, frozen in isopentane, and stored at −40°C. The brains were cut in 40 μm coronal sections in a Reichert-Jung cryostat (Leica Microsystems, Bannockburn, IL) at −17°C and collected onto glass slides. Two adjacent series were created for cytochrome oxidase and Nissl staining. The brains were stained for cytochrome oxidase quantitative enzyme histochemistry as described in detail previously (Gonzalez-

Lima and Cada, 1998; Gonzalez-Lima and Jones, 1994). All chemicals were purchased from Sigma (St. Louis, MO).

2.3.2 Metabolic mapping—Cytochrome oxidase activity was used as a marker of neuronal oxidative metabolic capacity (Hevner and Wong-Riley, 1989). Optical density (OD) of the stained brain sections were measured using a well-established densitometric analysis (Gonzalez-Lima and Cada, 1998). Brain sections were stained in parallel, and we controlled for stain intensities using two series of standards in each batch. The standards were made of sectioned brain homogenates of known enzymatic activity measured biochemically. The activity measured in the standards and the stained sections were linearly correlated in each batch with r's > 0.95. Bilateral PCC activity was analyzed throughout the rostro-caudal axis (−1.8 to −5.3 mm from Bregma) (Paxinos and Watson, 1997). We also analyzed limbic and extra-limbic brain regions that are anatomically connected to the PCC and have been proposed to mediate mnemonic functions of Papez's circuit (Papez, 1937; Vertes et al., 2001). Table 2 lists all regions (and name abbreviations).

2.3.3 Posterior cingulate/retrosplenial cortical lesion volume—Unbiased stereological estimates of the total PCC volume affected by cytochrome oxidase inhibition were obtained from digital images of cytochrome oxidase activity-stained brain sections using the Cavalieri principle (Rojas et al., 2009b). Area (A) and the average distance between designated sections (d) estimated the total lesion volume based on the formula $V_{PCC}=\Sigma A \times d$, where d=(T) × (number of designated sections − 1) × (number of series), and T is the distance between every designated section (240 m).

2.3.4 Posterior cingulate/retrosplenial cortical cell density—Neuronal and glial cell densities in the PCC were estimated with an unbiased optical disector stereological method in Nissl-stained sections from control (*n*=6), AZ (*n*=6), and AZ+MB (*n*=6) groups (Harding et al., 1994; Riha et al., 2008). Cells were differentiated based on morphological criteria. Cell density was defined as $Nv_{cells}=\Sigma Q-/\Sigma v_{(frame)}$, where ΣQ− is the sum of cell counts per sample and $\Sigma v_{(frame)}$ is the area of the unbiased counting frame (0.0396 mm^2, adjusted for 140X magnification) multiplied by the length of the analyzed region (d). The length was calculated as d=(No. of sections − 1) × No. of section series × section thickness.

2.4 Statistical analyses and computational modeling

2.4.1 Analysis of variance and covariance—Reference memory and locomotor activity were examined with ANOVA and repeated-measures ANOVA (day × group), respectively. Significant group differences were further tested with Dunnett- and Tukey-corrected pairwise comparisons. Between-group differences in regional cytochrome oxidase activity and cell counts were determined using ANOVA followed by tests for simple effects for each region of interest. Differences in lesion volume were determined with Tukey-corrected ANOVA. Within-group Pearson product-moment correlations were computed to analyze the covariance relationships between cytochrome oxidase activity in the PCC, other brain regions, behavioral scores and morphometric values (Nair and Gonzalez-Lima, 1999). For all tests an alpha level of .05 (two-tailed) was the criterion of statistical significance. All tests were performed using SPSS 11.5 software (SPSS, Inc., Chicago, IL).

2.4.2 Graph theory methods—Network *functional connectivity* was measured using the average connection densities, connectivity matching indices and clustering indices (Sporns, 2003). *Functional connectivity* is a specific term defined by the graph theory methods used in this paper, developed by Sporns. It refers to activity inter-correlations among regions (covariate measure) and not to individual regional activity (univariate measure). Pairwise correlations matrices based on cytochrome oxidase activity were built for one global

network (including 20 cortical, limbic and thalamic regions) and for three sub-networks: 1) thalamus (AD, AV, AM, DM, Rt, Rh, Re, LD and MD), 2) medial temporal lobe (Ent, Per, dg dorsal, dg ventral, CA3 dorsal, CA3 ventral, CA1 dorsal, CA1 ventral, and Sub), and 3) visuomotor loop (M2, GP, CPu, V2 lateral and V2 medial). The average connection density (κ_{den}) within each group was computed as the number of significant correlations divided by the total number of possible correlations (i.e., maximal number of connections). An entry was given a non-zero value if it corresponded to a significant correlation between two regions (i.e., nodes). The total number of possible connections for a particular sub-network was calculated as [(number of nodes)×(number of nodes−1)]/2. κ_{den} values were converted to standard scores based on κ_{den} values random matrices with values from each group. Significant functional connectivity within an experimental group was considered to be present if its standard score was > ± 2.0. The between-group PCC connectivity matching index ($m_{A,B}$) evaluated the amount of overlap in the PCC connection patterns between groups. It was calculated as the number of effective connections between the PCC and specific brain regions in one group (A) that also existed in another group (B), divided by the total number of possible PCC connections within a group. Finally, a clustering index (γ_n) for a region of interest (v) was computed as a ratio of the total number of significant pairwise correlations between neighbor regions of v and the total number of possible connections in the matrix for a particular network including region v. γ_n revealed the tendency of regions within a sub-network to form functionally coupled modules.

2.4.3 Structural equation modeling—Structural equation modeling assessed between-group differences in the *effective connectivity* within networks of interest (McIntosh and Gonzalez-Lima, 1991, 1994; Puga et al., 2007). *Effective connectivity* differs from *functional connectivity* in that it models covariance of activity via known anatomical connections (paths) among regions. Data- and theory-driven network models were built based on discriminant analyses of cytochrome oxidase activity and known anatomical connectivity. Interregional correlations were used to compute path coefficients *via* a process of iterative data fitting (LISREL, version 8.54, Scientific Software). The path coefficients represented directional influences between brain regions. An optimal solution was achieved in a model including the AM, PCC and the hippocampus (HC). HC data was the average of DG, CA3, CA1 and Sub values, which were combined to avoid colinearity. The model also included the V2 and RLi, which respectively represent extralimbic cortical and subcortical regions with major direct projections to the PCC. Between-group differences were determined with global goodness-of-fit statistics derived from a stacked model approach in which path coefficients in one version of the model were constrained to be equal between groups (null hypothesis) and compared to another version where the path coefficients were allowed to vary (alternative hypothesis).

3. RESULTS

3.1 Systemic MB prevented the memory deficits induced by infusion of AZ into the PCC

During the initial habituation trials one rat failed to reach the criterion of consuming at least 15 pellets in one trial and it was excluded from the study. During the first eight days of training, all rats learned the holeboard pattern ($F_{(7, 182)} = 20.99$, $p < .001$). There were no group differences in holeboard training within the first 8 days ($F_{(2, 26)} = 0.266$) or in the remaining 9–14 days of training ($F_{(2,24)} = 2.95$). In addition, there were no group differences in reference memory for the last day of training or in the maximal training score.

A probe trial to evaluate visuospatial reference memory in the holeboard task was carried out 24 hr after bilateral infusion of AZ into the PCC. The groups were significantly different in their memory of the previously-baited holeboard ($F_{(2,26)} = 6.7$, $p = .004$; Fig. 1). The

mean reference memory score in the AZ group (0.25 ± 0.02) was 16% lower than that of the control group (0.30 ± 0.01) (Dunnett $p = .05$). The effect size of AZ treatment was .97. In contrast, the mean reference memory score in the AZ+MB group (0.33 ± 0.01) was similar to control (Dunnett $p = .28$) and was 32% higher than that of the AZ group (Tukey $p = .003$) (Fig. 1). Compared to mean pre-lesion baseline reference memory scores during training, the AZ group showed a 36% decrease in memory in the probe trial, whereas the control group showed a decrease of 25% and the AZ+MB group showed an even smaller decrease of only 19% ($F_{(2,26)} = 3.5$, $p = .04$). Thus, MB was not only able to significantly prevent the decrease in the reference memory scores induced by AZ, but it also tended to improve memory compared to intact control animals. No other task-related variable biased the group differences observed in the probe trial. For example, there were no group differences in: 1) the number of initial or repeated nosepokes into previously baited holes or previously-nonbaited holes, 2) total entries into previously-baited or previously-nonbaited holes, 3) total overall entries, or 4) time to complete the task during the probe trial.

In the open field, all groups significantly decreased the amount of time performing short movement behaviors in the second trial as compared to the first trial ($F_{(1, 26)} = 63.89$, $p < .001$), which is an expected effect of context habituation. However, there was no effect of drug treatment on short movement time or number of rearings ($F_{(2, 26)} = 0.994$ and $F_{(2, 26)} = 0.853$, respectively). There was a significant group effect for ambulatory time ($F_{(2, 26)} = 3.66$, $p = .04$). However, post-hoc analysis did not reveal a significant between-group difference and the significant result of the omnibus test appeared to be due to a higher activity in the AZ-treated group before treatment (Table 1). Therefore, the effects of MB can be regarded as memory-specific and not attributed to unspecific changes in locomotor activity.

3.2 Systemic MB reduced the cortical lesion volume produced by AZ

The stereological measures of enzymatic inhibition produced by AZ around the injection sites provided a direct estimate of the effective amount injected. This was verified using both Nissl histology (morphological tissue damage) and enzyme histochemistry (functional enzyme inhibition). Representative images of the lesion volume, including injection sites, are shown for sections from each group stained for Nissl (Fig. 2) and cytochrome oxidase activity (Fig. 3). Figs. 2 and 3 illustrate that the effects on tissue damage and cytochrome oxidase inhibition produced by the injections were restricted to the PCC. There was a 20% reduction in the average lesion volume due to MB administration between AZ and AZ+MB groups (Fig. 4). After the sham surgery the PCC volume in the control group showed a lesion of 1.6 ± 0.96 mm^3. The overall lesion volume of the PCC and contiguous regions showing any degree of cytochrome oxidase inhibition was 68.4 ± 8 mm^3 in the AZ group (Tukey $p < .001$, compared to control), but only 54.8 ± 5 mm^3 in the AZ+MB group (Tukey $p < .001$, compared to control). There were no inter-hemispheric differences in the lesion volume in the two groups.

The lesion volume effects were observed despite evidence of cytochrome oxidase inhibition at the sites of AZ infusion in the PCC in both AZ-treated groups. Compared to controls, rats in both the AZ and AZ+MB groups showed significant mean decreases in PCC cytochrome oxidase activity at the injection sites of infusion (17% and 28%, respectively) ($F_{(2, 26)} = 14.82$, $p < .001$). The region of PCC cytochrome oxidase inhibition started at Bregma −1.80 mm and extended caudally, reaching the maximal point of inhibition in the dorsal PCC at Bregma −3.4 mm, with a reduction of about 20% in mean cytochrome oxidase activity compared to control in both groups.

The greatest morphological lesion effect was also found in the dorsal PCC (Fig. 5). In fact, the superficial PCC at this point of maximal cytochrome oxidase inhibition (Bregma −3.4

mm) showed remarkable neurodegeneration and gliosis. Compared to control, in the PCC there was a 76% reduction in neuronal density ($F_{(2, 15)} = 12.93$, $p = .001$) and a 2-fold increase in glial density ($F_{(2, 15)} = 7.314$, $p = .021$) in both the AZ and AZ+MB groups.

In addition, we evaluated the individual cytochrome oxidase activity of all the brain regions measured, including regions adjacent to the injection sites, which clearly showed that the AZ did not diffuse to other regions and only the PCC showed an inhibition of cytochrome oxidase activity (Table 2).

3.3 Systemic MB prevented the disruption in PCC effective connectivity

The memory-preserving effects of MB could be partially attributed to the prevention of structural damage (Fig. 2) and anatomical restriction of the extent of PCC cytochrome oxidase inhibition induced by AZ (Fig. 3). But as described above, systemic MB did not prevent the local decreases in cytochrome oxidase activity in the PCC caused by AZ. Nor where MB's behavioral effects due to absolute increases in cytochrome oxidase activity in other brain regions interconnected with the PCC, since a between-group analysis of cytochrome oxidase activity in those brain regions did not reveal significant differences (Table 2). In addition, whole-brain cytochrome oxidase activity was not different between the groups. It was noted that the connectivity density (κ_{den}) of the PCC was equally decreased in both AZ and the AZ+MB groups. For example, whereas the control group showed 12 significant interregional correlations of cytochrome oxidase activity between the PCC and 19 other brain regions ($\kappa_{den} = .63$), sodium azide reduced the total number of significant correlations between these regions in both AZ and AZ+MB groups ($\kappa_{den} = .36$ and $\kappa_{den} = .26$, respectively). Nevertheless, the PCC connectivity matching index between the AZ group and AZ+MB groups ($m_{AZ,AZ+MB}$) was zero, while the PCC connectivity matching index between the control and AZ+MB groups was higher than that between control and AZ groups ($m_{Control,AZ+MB} = 0.21$ and $m_{control,AZ} = 0.05$, respectively). In other words, the remaining functional network in the AZ+MB group after the PCC lesion was more similar to control than that of the AZ group. In particular, MB maintained the PCC functional network with the dorsal hippocampus proper and the secondary visual cortex, as observed in the control group (Fig. 6, Table 3). These data suggest that in addition to reducing structural damage to the PCC, the memory-preserving effects of MB are also due to preservation of the functional network between the PCC and key regions involved in the visuospatial memory task.

To test this hypothesis, we compared the system-level changes in effective connectivity in the control, AZ and AZ+MB groups by means of structural equation modeling. The cytochrome oxidase activity data derived from metabolic mapping were applied to a thalamo-cingulo-hippocampal network model resembling that proposed by Papez (1937). A significant control group model solution showed the PCC receiving the highest number of inputs and holding reciprocal connections with the anteromedial thalamic nucleus and the hippocampus (HC), and receiving negative influences from the secondary visual cortex (V2) and the raphe nuclei (RLi) (Fig. 7). Within this network, PCC cytochrome oxidase inhibition produced three major significant changes in effective connectivity that included: 1) path coefficient sign reversal of all PCC inputs and outputs (e.g., an input that suppressed the activity of the PCC in controls increased PCC activity in AZ-treated subjects); 2) strengthening of the thalamo-cingulate connectivity; and 3) remarkable recruitment of the raphe nuclei and secondary visual cortex, which provided strong positive influences on the PCC. In contrast, in the AZ+MB group, the path coefficient signs of PCC inputs and outputs were similar to control, except for that of the raphe nuclei, which continued exerting a positive influence on the PCC, as seen in the AZ group. Also, MB induced a strengthening of the influence of V2 on the PCC with a path coefficient sign similar to control and opposite to AZ. AZ+MB-treated subjects showed strong interactions between the PCC and

the thalamus, while the weak connectivity between the PCC and the HC, resembled that of the AZ group. Remarkably, an alternate output from the thalamus to the secondary visual cortex not involving the PCC remained unchanged in the three groups, indicating that the interventions were specific to regions of the Papez circuit. Effects not accounted for by the regions included in the model were expressed as residuals. The residuals for AM, HC, V2 and RLi ranged from .63 to 1.56, while the PCC showed comparatively lower residuals in the three groups (.21, .20 and .17 for control, AZ and AZ+MB, respectively). This signifies that the regions included in the model explain the majority of the effects observed in the PCC. Alternate models focusing on hippocampal connectivity but not including the PCC were unsolvable or did not show differences between groups (data not shown). The above evidence support that, whereas AZ induced a marked disruption in normal PCC effective connectivity, MB may exert its memory-preserving effects by partially restoring the functional network between the PCC and key limbic and extralimbic regions implicated in visuospatial memory.

3.4 Systemic MB altered the local functional network within thalamic, medial temporal lobe and visuomotor loop sub-networks

Although MB improved the effective connectivity of the PCC, it was also possible that the cognitive effects of MB were supplemented by facilitating local strategies for memory retrieval concomitant to the strengthening of PCC effective connectivity. To test this hypothesis, we analyzed the local functional network within the thalamus; the medial temporal lobe (MTL), including the hippocampus and parahippocampal region; and a visuomotor loop including the secondary motor (M2) and visual (V2) cortices, the striatum (CPu) and the globus pallidus (gp). PCC cytochrome oxidase inhibition prompted thalamic regions to associate functionally and share common networks, as indicated by a 25% increase in the thalamic average clustering index (γ_n) in the AZ group, compared to control (Dunnett, $p = .03$). No changes in γ_n were induced by AZ in the MTL or the visuomotor loop. In contrast, MB increased or decreased local clustering, depending on the local sub-network on which it acted. Fig. 8 shows that compared to control, MB induced a 27% decrease in the thalamus (Dunnett, $p = .02$), a 40% increase in the MTL (Dunnett, $p = .001$) and a 66% decrease in γ_n values in the visuomotor loop (Dunnett, $p = .04$). The efficacy of MB at preventing redundant local connectivity was highlighted by its induction of overall decreases in κ_{den} within the thalamus and the motor loop (Table 4). These data reveal that MB not only restored the original sub-network connectivity of the control group, but also enhanced local adaptive metabolic changes in brain sub-networks interconnected with the PCC.

4. DISCUSSION

This study provides evidence that a single systemic injection of 4 mg/kg USP methylene blue (MB) prevents the memory deficits secondary to PCC cytochrome oxidase inhibition induced by a local infusion of a mitochondrial inhibitor of cytochrome oxidase. Relevant to amnestic mild cognitive impairment, this experimental paradigm demonstrated meaningful MB behavioral effects that were accompanied by stereological evidence of neuroprotection. This is the first study to show that systemic MB administration prevented the structural and hypometabolic damage induced by a mitochondrial insult impairing energy metabolism. This study also presents evidence that MB induces brain circuit-specific changes in functional and effective connectivity, supporting a mechanism of action based on its metabolic-enhancing effects in the brain.

A number of considerations support the validity of the findings. First, PCC hypometabolism as measured by cytochrome oxidase inhibition was induced after the subjects learned the visuospatial task. Thus, the lesions did not interfere with encoding or sorting of visuospatial

information. Consequently, the post-lesion probe specifically tested how AZ and MB interfered with memory retrieval. In addition, neither AZ nor AZ+MB-treated rats were different from controls in exploratory activity in an open field chamber, and there were no group differences in activity or in the latency to complete the task during the probe trial. Therefore, the decreased performance in the memory task observed in the AZ group was not biased by the presence of psychomotor deficits. Neural cell density in the PCC at Bregma levels with the lowest cytochrome oxidase activity was significantly decreased in both AZ− and AZ+MB-treated animals as compared to controls. This decrease was accompanied by massive gliosis in both treatment groups. This supports that AZ exerted its neurotoxic effects in the presence of MB, and that MB did not act by displacing AZ from its binding site in cytochrome oxidase. Also, although MB is potentially available to all brain regions after systemic administration, its mechanism of action cannot be explained by a global and non-specific increase in brain metabolic activity. The network effects are the result of differences in the inter-regional correlations of activity produced by the modified influence from the affected PCC, not the result of enzyme inhibition by AZ in other regions, as none of the regions outside of the injected PCC showed a change of enzymatic activity. Functional changes appeared to mainly involve the PCC and the regions holding direct anatomical interactions with it. For example, an effective connection between the thalamus and the secondary visual cortex was not altered by AZ or MB, and was thus probably not as crucial for the completion of the memory task. Furthermore, PCC residuals in the structural equation model tended to be low, signifying that the regions included in the model explain most of the activity in the PCC. The different patterns of effective connectivity between the AZ and AZ+MB groups indicate that the behavioral changes elicited by MB can be explained by its effects in these specific regions. The data support that the metabolic effects of MB were contingent upon the neural context within the circuit of Papez and that MB can boost coherent and orchestrated metabolic adaptations in response to physical alterations to the networks involved in visuospatial memory.

A major finding of this study is that MB preserved the thalamo-cingulo-hippocampal effective connectivity. This is illustrated by the similarity between control and AZ+MB groups, and their differences with the AZ group. We used structural equation modeling to assess the changes in effective connectivity underlying the memory-improving effects of MB. This strategy was selected because of its high power for identifying group differences that would otherwise be unrevealed by univariate statistical comparisons. In this modeling approach, the network connectivity is based on regional effective (i.e., directional) interactions that determine the magnitude and sign of the covariance in activity patterns (McIntosh and Gonzalez-Lima, 1991; Sakata et al., 2000). A major disadvantage of this technique is that it is non-temporal and offers a rather static view of connectivity patterns. However, this is compensated by the use of quantitative cytochrome oxidase histochemical activity data. This histochemical method reflects the capacity for the holoenzyme to change its catalytic activity in response to neuronal energy demands over a period of time (Gonzalez-Lima and Jones, 1994). Thus, it provides a historical account of tissue changes in metabolic demand for oxidative energy. Structural equation models based on cytochrome oxidase activity express how a change in cytochrome oxidase activity in a specific region is associated with an increase or decrease of cytochrome oxidase activity in another region (Puga et al., 2007). This provides not only an overview of the functional coupling between regions in terms of energy-dependent oxidative metabolic capacity, but it also gives insight into the directionality of influences (e.g., what region within the network drives the metabolic changes in other regions within that network). The combination of these methods is sensitive to brain metabolic changes associated with learning and behavior expression (Puga et al., 2007; Sakata et al., 2000).

Our results support previous studies showing that the PCC is a crucial region for visuospatial memory and a major point of metabolic vulnerability for the onset of neurodegenerative disorders characterized by visuospatial memory impairment. Extensive network analyses have identified the PCC as one of the main connector hubs in the brain, playing a pivotal role in the coordination of information flow (Sporns et al., 2007). The PCC is not only a complex and highly interconnected brain region, but it also has direct anatomical connections to numerous brain regions and constitutes a major building block of the "default mode" network (Fransson and Marrelec, 2008). The pathophysiologic relevance of PCC dysfunction has been widely documented in clinical studies (Valenstein et al., 1987). The PCC is part of a constant hypometabolic cluster in patients with MCI who later convert to AD (Morbelli et al., 2010; Nobili et al., 2008; Pagani et al., 2009). Patients with MCI also show PCC hypoperfusion associated with decreased memory performance (Chao et al., 2009), and decreased oxygen consumption during encoding and retrieval (Machulda et al., 2009). Abnormalities in PCC function can be detected in cognitively intact adults with a family history of AD or ApoE4 carriership under resting-state conditions (Reiman et al., 2001) and during semantic memory tasks (Seidenberg et al., 2009). In fact, individuals who are ApoE4 carriers or have family history of AD have a decreased risk of AD if they show normal PCC metabolism during performance of memory tasks (Xu et al., 2009). PCC perfusion is positively correlated with MTL volume in aMCI (Guedj et al., 2009), and PCC atrophy can be found in aMCI and early AD (Pa et al., 2009; Shiino et al., 2008). From the neural-network perspective, it has been previously predicted that lesions in connector hubs, such as the PCC, will increase the small-world index of a network due to increases in path length (Sporns et al., 2007).

We showed that isolated PCC cytochrome oxidase inhibition caused visuospatial memory deficits that were mediated by a weakening of the cingulo-hippocampal connectivity and a strengthening of the cingulo-thalamic effective connectivity. At the same time, the local connectivity between thalamic regions increased after the lesions. Together, these data support the role of the PCC as a major connector hub in the brain. Interventions that promote a robust PCC connectivity might be effective at preventing memory deficits in patients with aMCI or other conditions associated with PCC hypometabolism.

We demonstrated that MB was highly effective at preventing the memory deficits induced by PCC cytochrome oxidase inhibition. In addition to partially preventing the acute neurodegenerative effects of AZ, MB also induced distinctive functional effects at the brain systems level, supporting its role as a metabolic enhancer. Pharmaceutical grade (USP) methylene blue is an FDA-grandfathered drug with powerful antioxidant activity approved for the treatment of methemoglobinemia (Bradberry, 2003). While chemical grade methylene blue is an industrial dye that may contain contaminants with potential toxicity (Auerbach et al., 2010), purified pharmaceutical grade MB used at low doses has no toxic effects in humans (Bradberry, 2003; Naylor et al., 1986; Naylor et al., 1987) and is well-documented for enhancing memory at the 4 mg/kg dose used in the present study (Bruchey and Gonzalez-Lima, 2008; Gonzalez-Lima and Bruchey, 2004; Martinez Jr. et al., 1978; Riha et al., 2005; Wrubel et al., 2007a; 2007b). The specificity of the brain metabolic changes and memory-enhancing effects induced by MB can be explained by both its pharmacokinetic and pharmacodynamic properties. MB readily crosses the blood-brain barrier and has wide central nervous system bioavailability (Peter et al., 2000; Walter-Sack et al., 2009). It has affinity for tissues with high aerobic metabolic rates, such as the brain (Peter et al., 2000), which has prompted its use as a supravital stain in the brain and other tissues (Muller, 1998). Its electrochemical properties confer it affinity for oxidoreductases and thus, it concentrates in mitochondria where it mimics the activity of membrane-embedded respiratory chain electron carriers (Scott and Hunter, 1966). MB restores inhibition of oxygen consumption caused by rotenone, an inhibitor of the first enzyme in the

mitochondrial electron transport chain (Lindahl and Oberg, 1961; Zhang et al., 2006), and MB stimulates cellular respiration in rat liver (Visarius et al., 1997) and brain (Riha et al., 2005; Zhang et al., 2006). Also, MB prevents the depletion in retinal and striatal metabolic capacity induced by mitochondrial inhibition (Rojas et al., 2009a; 2009b). Thus, an important consideration for the proposed mechanism of action of MB is that although its distribution in the brain is potentially universal, its action as a metabolic enhancer is dictated by the metabolic rate of neurons in a particular brain region. Regions with a higher metabolic requirement due to cognitive demands (e.g., undergoing activation or subjected to metabolic stress) will concentrate MB and selectively increase their energy metabolism (Gonzalez-Lima and Bruchey, 2004). Primarily in these regions, MB will enhance electron transport, oxygen consumption and energy formation, thus improving their metabolic performance and facilitating their contributions to network function preservation. In this pharmacokinetic sense, MB displays the attributes of the 'magic bullet' originally theorized by Paul Ehrlich (Gensini et al., 2007). In addition, MB belongs to a group of chemicals with the most potent known antioxidant properties (Moosmann et al., 2001). It decreases free radical formation during reperfusion after ischemia (Kelner and Alexander, 1985; Salaris et al., 1991), lipid peroxidation (Visarius et al., 1999; Zhang et al., 2006) and superoxide formation secondary to mitochondrial inhibition in the brain parenchyma (Rojas et al., 2009b). In fact, MB's *in vivo* neuroprotective effects against acute ischemia/reperfusion injury are related to the inhibition of both cerebral and systemic nitroxidative stress (Miclescu, 2009; Miclescu et al., 2006, 2007). Thus, compelling evidence supports that MB is able to provide biologically meaningful neuroprotective effects, which are evident as preservation of neural structure and function *in vivo*. Such effects appear to be linked to its peculiar bioenergetically-driven bioavailability in the brain and its dual profile as an antioxidant and metabolic-enhancing agent (Furian et al., 2007; Rojas and Gonzalez-Lima, 2010; Rojas et al., 2009a; 2009b; Wiklund et al., 2007; Zhang et al., 2006).

5. CONCLUSION

Systemic MB enhances memory function and is able to prevent network-level disruptions in brain oxidative metabolic capacity. MB is a candidate drug with potential to effectively treat memory deficits in patients with cognitive impairment characterized by PCC cytochrome oxidase inhibition. Due to its neuroprotective effects, MB could also have disease-modifying effects in AD and neurodegenerative conditions featuring abnormal brain oxidative energy metabolism and memory function. The findings support studies of mitochondrial contributions to neurodegenerative diseases, including the azide model of AD (Bennett et al., 1992) and ongoing clinical trials using MB for AD (Wischik and Staff, 2009).

Research highlights

- Methylene blue (MB) improves memory in a model of mild cognitive impairment (MCI)
- MB reduces the lesion volume induced by posterior cingulate hypometabolism
- MB normalizes the effective connectivity of the posterior cingulate cortex
- MB modifies network functional connectivity within the circuit of Papez
- This is the first study of MB's beneficial effects in a model of amnestic MCI

Acknowledgments

We would like to thank Christian Balderrama for his help in tissue processing and Douglas Barrett for assisting in the brain composition figure. Supported in part by NIH grants MH076847 and MH65728 to FGL.

References

Auerbach SS, Bristol DW, Peckham JC, Travlos GS, Hebert CD, Chhabra RS. Toxicity and carcinogenicity studies of methylene blue trihydrate in F344N rats and B6C3F1 mice. Food Chem Toxicol. 2010; 48:169–177. [PubMed: 19804809]

Bennett MC, Diamond DM, Stryker SL, Parks JK, Parker WD Jr. Cytochrome oxidase inhibition: a novel animal model of Alzheimer's disease. J Geriatr Psychiatry Neurol. 1992; 5:93–101. [PubMed: 1317179]

Bennett MC, Rose GM. Chronic sodium azide treatment impairs learning of the Morris water maze task. Behav Neural Biol. 1992; 58:72–75. [PubMed: 1417674]

Bradberry SM. Occupational methaemoglobinaemia. Mechanisms of production, features, diagnosis and management including the use of methylene blue. Toxicol Rev. 2003; 22:13–27. [PubMed: 14579544]

Bruchey AK, Gonzalez-Lima F. Behavioral, physiological and biochemical hormetic responses to the autoxidizable dye methylene blue. Am J Pharm & Toxicol. 2008; 3:69–76.

Bussey TJ, Muir JL, Everitt BJ, Robbins TW. Dissociable effects of anterior and posterior cingulate cortex lesions on the acquisition of a conditional visual discrimination: facilitation of early learning vs. impairment of late learning. Behav Brain Res. 1996; 82:45–56. [PubMed: 9021069]

Callaway NL, Riha PD, Bruchey AK, Munshi Z, Gonzalez-Lima F. Methylene blue improves brain oxidative metabolism and memory retention in rats. Pharmacol Biochem Behav. 2004; 77:175–181. [PubMed: 14724055]

Callaway NL, Riha PD, Wrubel KM, McCollum D, Gonzalez-Lima F. Methylene blue restores spatial memory retention impaired by an inhibitor of cytochrome oxidase in rats. Neurosci Lett. 2002; 332:83–86. [PubMed: 12384216]

Chao LL, Pa J, Duarte A, Schuff N, Weiner MW, Kramer JH, Miller BL, Freeman KM, Johnson JK. Patterns of cerebral hypoperfusion in amnestic and dysexecutive MCI. Alzheimer Dis Assoc Disord. 2009; 23:245–252. [PubMed: 19812467]

Chetelat G, Desgranges B, de la Sayette V, Viader F, Eustache F, Baron JC. Mild cognitive impairment: Can FDG-PET predict who is to rapidly convert to Alzheimer's disease? Neurology. 2003; 60:1374–1377. [PubMed: 12707450]

Drzezga A, Lautenschlager N, Siebner H, Riemenschneider M, Willoch F, Minoshima S, Schwaiger M, Kurz A. Cerebral metabolic changes accompanying conversion of mild cognitive impairment into Alzheimer's disease: a PET follow-up study. Eur J Nucl Med Mol Imaging. 2003; 30:1104–1113. [PubMed: 12764551]

Fransson P, Marrelec G. The precuneus/posterior cingulate cortex plays a pivotal role in the default mode network: Evidence from a partial correlation network analysis. Neuroimage. 2008; 42:1178–1184. [PubMed: 18598773]

Furian AF, Fighera MR, Oliveira MS, Ferreira AP, Fiorenza NG, de Carvalho Myskiw J, Petry JC, Coelho RC, Mello CF, Royes LF. Methylene blue prevents methylmalonate-induced seizures and oxidative damage in rat striatum. Neurochem Int. 2007; 50:164–171. [PubMed: 16963161]

Gensini GF, Conti AA, Lippi D. The contributions of Paul Ehrlich to infectious disease. J Infect. 2007; 54:221–224. [PubMed: 16567000]

Gonzalez-Lima F, Bruchey AK. Extinction memory improvement by the metabolic enhancer methylene blue. Learn Mem. 2004; 11:633–640. [PubMed: 15466319]

Gonzalez-Lima, F.; Cada, A. Quantitative histochemistry of cytochrome oxidase activity: Theory, methods, and regional brain vulnerability. In: Gonzalez-Lima, F., editor. Cytochrome oxidase in neuronal metabolism and Alzheimer's disease. Plenum press; New York: 1998. p. 55-90.

Gonzalez-Lima F, Jones D. Quantitative mapping of cytochrome oxidase activity in the central auditory system of the gerbil: a study with calibrated activity standards and metal-intensified histochemistry. Brain Res. 1994; 660:34–49. [PubMed: 7828000]

Gonzalez-Lima, F.; Valla, J.; Jorandby, L. Cytochrome oxidase inhibition in Alzheimer's disease. In: Gonzalez-Lima, F., editor. Cytochrome Oxidase in Neuronal Metabolism and Alzheimer's Disease. Plenum Press; New York: 1998. p. 171-201.

Guedj E, Barbeau EJ, Didic M, Felician O, de Laforte C, Ranjeva JP, Poncet M, Cozzone PJ, Mundler O, Ceccaldi M. Effects of medial temporal lobe degeneration on brain perfusion in amnestic MCI of AD type: deafferentation and functional compensation? Eur J Nucl Med Mol Imaging. 2009; 36:1101–1112. [PubMed: 19224210]

Harding AJ, Halliday GM, Cullen K. Practical considerations for the use of the optical disector in estimating neuronal number. J Neurosci Methods. 1994; 51:83–89. [PubMed: 8189753]

Hevner RF, Wong-Riley MT. Brain cytochrome oxidase: purification, antibody production, and immunohistochemical/histochemical correlations in the CNS. J Neurosci. 1989; 9:3884–3898. [PubMed: 2555458]

Jagust WJ, Landau SM, Shaw LM, Trojanowski JQ, Koeppe RA, Reiman EM, Foster NL, Petersen RC, Weiner MW, Price JC, Mathis CA. Relationships between biomarkers in aging and dementia. Neurology. 2009; 73:1193–1199. [PubMed: 19822868]

Johnson DK, Storandt M, Morris JC, Galvin JE. Longitudinal study of the transition from healthy aging to Alzheimer disease. Arch Neurol. 2009; 66:1254–1259. [PubMed: 19822781]

Kelner MJ, Alexander NM. Methylene blue directly oxidizes glutathione without the intermediate formation of hydrogen peroxide. J Biol Chem. 1985; 260:15168–15171. [PubMed: 4066667]

Lindahl PE, Oberg KE. The effect of rotenone on respiration and its point of attack. Exp Cell Res. 1961; 23:228–237. [PubMed: 13762256]

Machulda MM, Senjem ML, Weigand SD, Smith GE, Ivnik RJ, Boeve BF, Knopman DS, Petersen RC, Jack CR. Functional magnetic resonance imaging changes in amnestic and nonamnestic mild cognitive impairment during encoding and recognition tasks. J Int Neuropsychol Soc. 2009; 15:372–382. [PubMed: 19402923]

Martinez JL Jr, Jensen RA, Vasquez BJ, McGuinness T, McGaugh JL. Methylene blue alters retention of inhibitory avoidance responses. Physiological Psychology. 1978; 6:387–390.

McIntosh AR, Gonzalez-Lima F. Structural modeling of functional neural pathways mapped with 2-deoxyglucose: effects of acoustic startle habituation on the auditory system. Brain Res. 1991; 547:295–302. [PubMed: 1884204]

McIntosh AR, Gonzalez-Lima F. Structural equation modeling and its application to network analysis in functional brain imaging. Hum Brain Mapp. 1994; 2:2–22.

Miclescu, A. Acta Universitatis Upsaliensis. Uppsala University; Uppsala: 2009. Cerebral protection in experimental cardiopulmonary resuscitation with special reference to the effects of methylene blue.

Miclescu A, Basu S, Wiklund L. Methylene blue added to a hypertonic-hyperoncotic solution increases short-term survival in experimental cardiac arrest. Crit Care Med. 2006; 34:2806–2813. [PubMed: 16957637]

Miclescu A, Basu S, Wiklund L. Cardio-cerebral and metabolic effects of methylene blue in hypertonic sodium lactate during experimental cardiopulmonary resuscitation. Resuscitation. 2007; 75:88–97. [PubMed: 17482336]

Minoshima S, Giordani B, Berent S, Frey KA, Foster NL, Kuhl DE. Metabolic reduction in the posterior cingulate cortex in very early Alzheimer's disease. Ann Neurol. 1997; 42:85–94. [PubMed: 9225689]

Moosmann B, Skutella T, Beyer K, Behl C. Protective activity of aromatic amines and imines against oxidative nerve cell death. Biol Chem. 2001; 382:1601–1612. [PubMed: 11767950]

Morbelli S, Piccardo A, Villavecchia G, Dessi B, Brugnolo A, Piccini A, Caroli A, Frisoni G, Rodriguez G, Nobili F. Mapping brain morphological and functional conversion patterns in amnestic MCI: a voxel-based MRI and FDG-PET study. Eur J Nucl Med Mol Imaging. 2010; 37:36–45. [PubMed: 19662411]

Mosconi L. Brain glucose metabolism in the early and specific diagnosis of Alzheimer's disease. FDG-PET studies in MCI and AD. Eur J Nucl Med Mol Imaging. 2005; 32:486–510. [PubMed: 15747152]

Mosconi L, Mistur R, Switalski R, Brys M, Glodzik L, Rich K, Pirraglia E, Tsui W, De Santi S, de Leon MJ. Declining brain glucose metabolism in normal individuals with a maternal history of Alzheimer disease. Neurology. 2009; 72:513–520. [PubMed: 19005175]

Mosconi L, Pupi A, De Leon MJ. Brain glucose hypometabolism and oxidative stress in preclinical Alzheimer's disease. Ann N Y Acad Sci. 2008; 1147:180–195. [PubMed: 19076441]

Mosconi L, Sorbi S, de Leon MJ, Li Y, Nacmias B, Myoung PS, Tsui W, Ginestroni A, Bessi V, Fayyazz M, Caffarra P, Pupi A. Hypometabolism exceeds atrophy in presymptomatic early-onset familial Alzheimer's disease. J Nucl Med. 2006; 47:1778–1786. [PubMed: 17079810]

Muller T. Methylene blue supravital staining: an evaluation of its applicability to the mammalian brain and pineal gland. Histol Histopathol. 1998; 13:1019–1026. [PubMed: 9810498]

Nair HP, Gonzalez-Lima F. Extinction of behavior in infant rats: development of functional coupling between septal, hippocampal, and ventral tegmental regions. J Neurosci. 1999; 19:8646–8655. [PubMed: 10493765]

Naylor GJ, Martin B, Hopwood SE, Watson Y. A two-year double-blind crossover trial of the prophylactic effect of methylene blue in manic-depressive psychosis. Biol Psychiatry. 1986; 21:915–920. [PubMed: 3091097]

Naylor GJ, Smith AH, Connelly P. A controlled trial of methylene blue in severe depressive illness. Biol Psychiatry. 1987; 22:657–659. [PubMed: 3555627]

Nobili F, Salmaso D, Morbelli S, Girtler N, Piccardo A, Brugnolo A, Dessi B, Larsson SA, Rodriguez G, Pagani M. Principal component analysis of FDG PET in amnestic MCI. Eur J Nucl Med Mol Imaging. 2008; 35:2191–2202. [PubMed: 18648805]

Pa J, Boxer A, Chao LL, Gazzaley A, Freeman K, Kramer J, Miller BL, Weiner MW, Neuhaus J, Johnson JK. Clinical-neuroimaging characteristics of dysexecutive mild cognitive impairment. Ann Neurol. 2009; 65:414–423. [PubMed: 19399879]

Pagani, M.; Dessi, B.; Morbelli, S.; Brugnolo, A.; Salmaso, D.; Piccini, A.; Mazzei, D.; Villavecchia, G.; Larsson, SA.; Rodriguez, G.; Nobili, F. MCI Patients Declining and Not-Declining at Mid-Term Follow-up: FDG-Pet Findings. Curr Alzheimer Res. 2009. In press (originally published online Nov. 26, 2009, at http://www.benthamdirect.org/pages/b_viewarticle.php?3159264)

Papez JW. A proposed mechanism of emotion. Arch Neurol Psychiatry. 1937; 38:725–743.

Paxinos, G.; Watson, C. The Rat Brain in Stereotaxic Coordinates. Academic Press; San Diego: 1997.

Peter C, Hongwan D, Kupfer A, Lauterburg BH. Pharmacokinetics and organ distribution of intravenous and oral methylene blue. Eur J Clin Pharmacol. 2000; 56:247–250. [PubMed: 10952480]

Puga F, Barrett DW, Bastida CC, Gonzalez-Lima F. Functional networks underlying latent inhibition learning in the mouse brain. Neuroimage. 2007; 38:171–183. [PubMed: 17703956]

Reiman EM, Caselli RJ, Chen K, Alexander GE, Bandy D, Frost J. Declining brain activity in cognitively normal apolipoprotein E epsilon 4 heterozygotes: A foundation for using positron emission tomography to efficiently test treatments to prevent Alzheimer's disease. Proc Natl Acad Sci USA. 2001; 98:3334–3339. [PubMed: 11248079]

Reiman EM, Uecker A, Gonzalez-Lima F, Minear D, Chen K, Callaway NL, Berndt JD, Games D. Tracking Alzheimer's disease in transgenic mice using fluorodeoxyglucose autoradiography. Neuroreport. 2000; 11:987–991. [PubMed: 10790869]

Riha PD, Bruchey AK, Echevarria DJ, Gonzalez-Lima F. Memory facilitation by methylene blue: dose-dependent effect on behavior and brain oxygen consumption. Eur J Pharmacol. 2005; 511:151–158. [PubMed: 15792783]

Riha PD, Rojas JC, Colorado RA, Gonzalez-Lima F. Animal model of posterior cingulate cortex hypometabolism implicated in amnestic MCI and AD. Neurobiol Learn Mem. 2008; 90:112–124. [PubMed: 18316212]

Rojas JC, Gonzalez-Lima F. Mitochondrial optic neuropathy: In vivo model of neurodegeneration and neuroprotective strategies. Eye and Brain. 2010; 2:21–37.

Rojas JC, John JM, Lee J, Gonzalez-Lima F. Methylene blue provides behavioral and metabolic neuroprotection against optic neuropathy. Neurotox Res. 2009a; 15:260–273. [PubMed: 19384599]

Rojas JC, Simola N, Kermath BA, Kane JR, Schallert T, Gonzalez-Lima F. Striatal neuroprotection with methylene blue. Neuroscience. 2009b; 163:877–889. [PubMed: 19596056]

Sakata JT, Coomber P, Gonzalez-Lima F, Crews D. Functional connectivity among limbic brain areas: differential effects of incubation temperature and gonadal sex in the leopard gecko, Eublepharis macularius. Brain Behav Evol. 2000; 55:139–151. [PubMed: 10899708]

Salaris SC, Babbs CF, Voorhees WD 3rd. Methylene blue as an inhibitor of superoxide generation by xanthine oxidase. A potential new drug for the attenuation of ischemia/reperfusion injury. Biochem Pharmacol. 1991; 42:499–506. [PubMed: 1650213]

Scott A, Hunter FE Jr. Support of thyroxine-induced swelling of liver mitochondria by generation of high energy intermediates at any one of three sites in electron transport. J Biol Chem. 1966; 241:1060–1066. [PubMed: 5933864]

Seidenberg M, Guidotti L, Nielson KA, Woodard JL, Durgerian S, Antuono P, Zhang Q, Rao SM. Semantic memory activation in individuals at risk for developing Alzheimer disease. Neurology. 2009; 73:612–620. [PubMed: 19704080]

Shiino A, Watanabe T, Kitagawa T, Kotani E, Takahashi J, Morikawa S, Akiguchi I. Different atrophic patterns in early- and late-onset Alzheimer's disease and evaluation of clinical utility of a method of regional z-score analysis using voxel-based morphometry. Dement Geriatr Cogn Disord. 2008; 26:175–186. [PubMed: 18698140]

Sporns, O. Graph theory methods for the analysis of neural connectivity patterns. In: Kotter, R., editor. Neuroscience databases. Kluwer Academic Publishers; Norwell: 2003.

Sporns O, Honey CJ, Kotter R. Identification and classification of hubs in brain networks. PLoS One. 2007; 2:e1049. [PubMed: 17940613]

Swerdlow RH, Parks JK, Cassarino DS, Maguire DJ, Maguire RS, Bennett JP Jr, Davis RE, Parker WD Jr. Cybrids in Alzheimer's disease: a cellular model of the disease? Neurology. 1997; 49:918–925. [PubMed: 9339668]

Valenstein E, Bowers D, Verfaellie M, Heilman KM, Day A, Watson RT. Retrosplenial amnesia. Brain. 1987; 110:1631–1646. [PubMed: 3427404]

Valla J, Berndt JD, Gonzalez-Lima F. Energy hypometabolism in posterior cingulate cortex of Alzheimer's patients: superficial laminar cytochrome oxidase associated with disease duration. J Neurosci. 2001; 21:4923–4930. [PubMed: 11425920]

Valla J, Schneider L, Reiman EM. Age- and transgene-related changes in regional cerebral metabolism in PSAPP mice. Brain Res. 2006; 1116:194–200. [PubMed: 16942758]

Vann SD, Aggleton JP. Extensive cytotoxic lesions of the rat retrosplenial cortex reveal consistent deficits on tasks that tax allocentric spatial memory. Behav Neurosci. 2002; 116:85–94. [PubMed: 11895186]

Vertes RP, Albo Z, Viana Di Prisco G. Theta-rhythmically firing neurons in the anterior thalamus: implications for mnemonic functions of Papez's circuit. Neuroscience. 2001; 104:619–625. [PubMed: 11440795]

Visarius TM, Stucki JW, Lauterburg BH. Stimulation of respiration by methylene blue in rat liver mitochondria. FEBS Lett. 1997; 412:157–160. [PubMed: 9257711]

Visarius TM, Stucki JW, Lauterburg BH. Inhibition and stimulation of long-chain fatty acid oxidation by chloroacetaldehyde and methylene blue in rats. J Pharmacol Exp Ther. 1999; 289:820–824. [PubMed: 10215658]

Wainwright M, Crossley KB. Methylene Blue--a therapeutic dye for all seasons? J Chemother. 2002; 14:431–443. [PubMed: 12462423]

Walter-Sack I, Rengelshausen J, Oberwittler H, Burhenne J, Mueller O, Meissner P, Mikus G. High absolute bioavailability of methylene blue given as an aqueous oral formulation. Eur J Clin Pharmacol. 2009; 65:179–189. [PubMed: 18810398]

Whishaw IQ, Maaswinkel H, Gonzalez CL, Kolb B. Deficits in allothetic and idiothetic spatial behavior in rats with posterior cingulate cortex lesions. Behav Brain Res. 2001; 118:67–76. [PubMed: 11163635]

Wiklund L, Basu S, Miclescu A, Wiklund P, Ronquist G, Sharma HS. Neuro- and cardioprotective effects of blockade of nitric oxide action by administration of methylene blue. Ann NY Acad Sci. 2007; 1122:231–244. [PubMed: 18077576]

Wischik C, Staff R. Challenges in the conduct of disease-modifying trials in Alzheimer's disease: practical experience from a phase 2 trial of TAU-aggregation inhibitor therapy. Journal of Nutrition Health and Aging. 2009; 13:367–369.

Wong-Riley MT. Cytochrome oxidase: an endogenous metabolic marker for neuronal activity. Trends Neurosci. 1989; 12:94–101. [PubMed: 2469224]

Wrubel KM, Barrett D, Shumake J, Johnson SE, Gonzalez-Lima F. Methylene blue facilitates the extinction of fear in an animal model of susceptibility to learned helplessness. Neurobiol Learn Mem. 2007a; 87:209–217. [PubMed: 17011803]

Wrubel KM, Riha PD, Maldonado MA, McCollum D, Gonzalez-Lima F. The brain metabolic enhancer methylene blue improves discrimination learning in rats. Pharmacol Biochem Behav. 2007b; 86:712–717. [PubMed: 17428524]

Xu G, McLaren DG, Ries ML, Fitzgerald ME, Bendlin BB, Rowley HA, Sager MA, Atwood C, Asthana S, Johnson SC. The influence of parental history of Alzheimer's disease and apolipoprotein E epsilon4 on the BOLD signal during recognition memory. Brain. 2009; 132:383–391. [PubMed: 18829694]

Zhang X, Rojas JC, Gonzalez-Lima F. Methylene blue prevents neurodegeneration caused by rotenone in the retina. Neurotox Res. 2006; 9:47–57. [PubMed: 16464752]

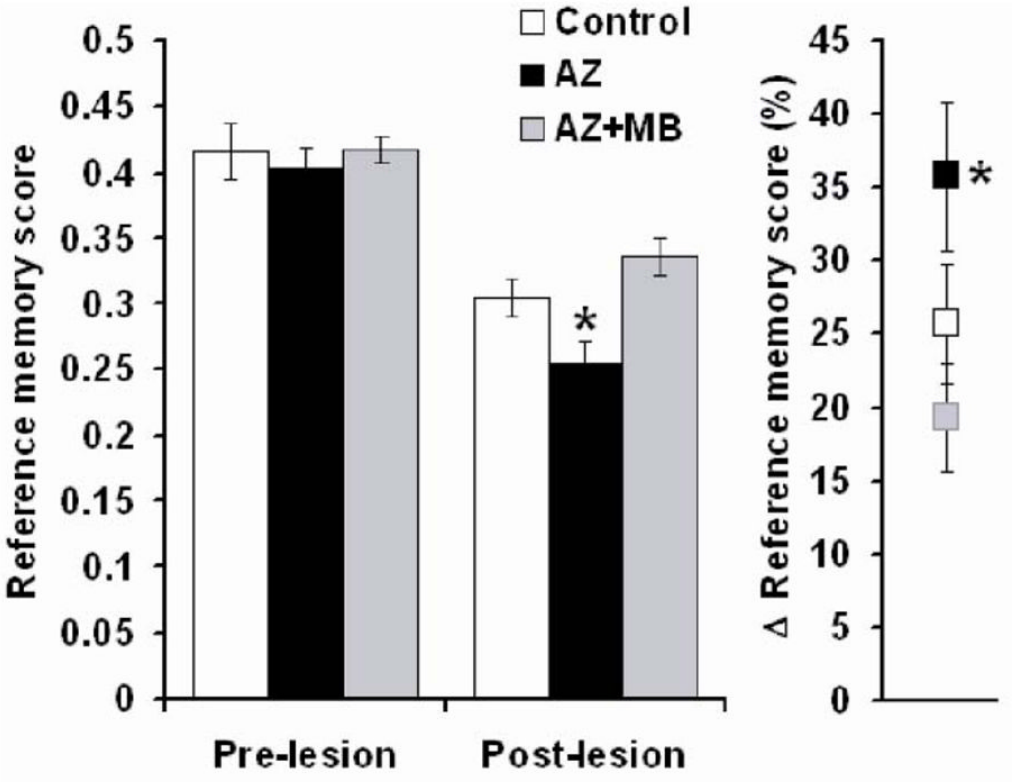

Figure 1. Systemic MB prevented the deficit in visospatial memory induced by PCC cytochrome oxidase inhibition

A) The average reference memory score at the end of training and before the PCC lesion was comparable between the three experimental groups. In the post-lesion probe, the three groups had a decreased reference memory compared to pre-lesion conditions. However, after the lesion, the reference memory score in the azide (AZ) group was significantly lower than sham control, whereas no deficit was observed in the AZ group treated with methylene blue (AZ+MB). B) The AZ group also showed the highest percent decrease () in the mean reference memory score, compared to baseline. * = significantly different from control, $p < 0.05$.

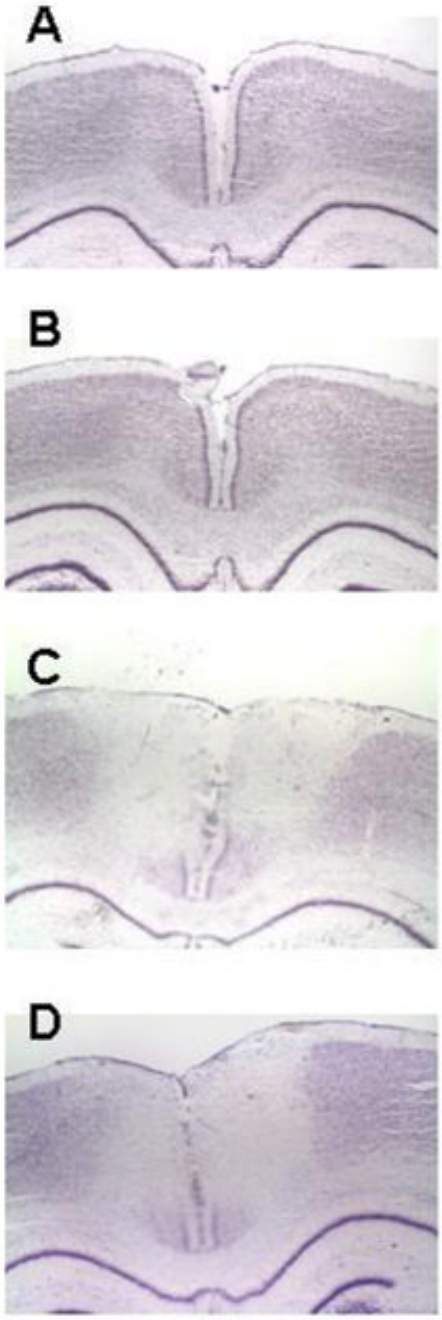

Figure 2. Systemic MB reduced the size of the histological damage produced by AZ

Representative photomicrographs of comparable Nissl-stained sections at the level of the AZ injection sites in the PCC to illustrate primary histological data. A) Control brain. Section from a sham operated rat not receiving any injections into the PCC, illustrating normal histology. B) Control vehicle-injected brain. Section from a sham operated rat receiving bilateral vehicle injections into the PCC, illustrating minimal effects on the histology. C) AZ injected brain. Section from an operated rat that received bilateral AZ injections into the PCC, illustrating discoloration and tissue damage on the PCC histology. D) AZ+MB injected brain. Section from an operated rat that received bilateral AZ injections into the PCC plus systemic MB, illustrating attenuated AZ effects on the histology of the PCC.

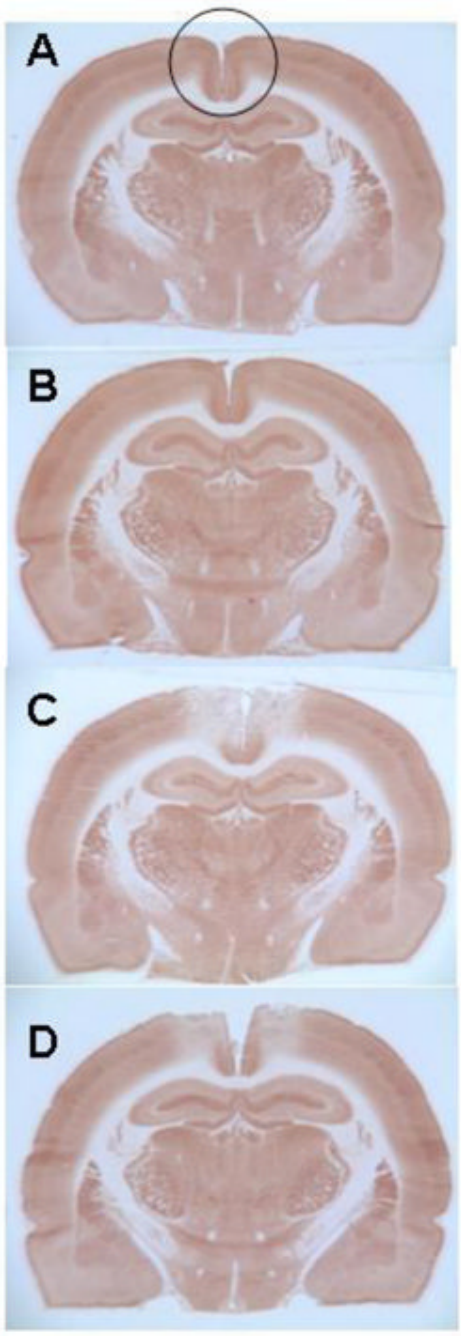

Figure 3. Systemic MB reduced the metabolic lesion in the PCC produced by AZ

Representative photomicrographs of comparable cytochrome oxidase histochemistry-stained sections at the level of the AZ injection sites in the PCC to illustrate primary histochemical data. The photomicrographs show entire sections to illustrate that the inhibition of cytochrome oxidase activity produced by AZ injections was limited to the PCC (area inside the circle) and did not involve other regions. Sections from each group were stained in parallel and the darkness (optical density) of the stained tissue was directly proportional to its cytochrome oxidase activity, as calibrated in each staining batch with tissue standards of known enzymatic activity measured biochemically (for histochemistry details refer to Gonzalez-Lima and Cada, 1998). A) Control brain. Section from a sham operated rat not

receiving any injections into the PCC, illustrating normal cytochrome oxidase histochemistry. B) Control vehicle-injected brain. Section from a sham operated rat receiving bilateral vehicle injections into the PCC, illustrating minimal effects on the cytochrome oxidase histochemistry. C) AZ injected brain. Section from an operated rat that received bilateral AZ injections into the PCC, illustrating reduced cytochrome oxidase histochemical activity in the PCC. D) AZ+MB injected brain. Section from an operated rat that received bilateral AZ injections into the PCC plus systemic MB, illustrating attenuated AZ effects on the cytochrome oxidase histochemical activity of the PCC.

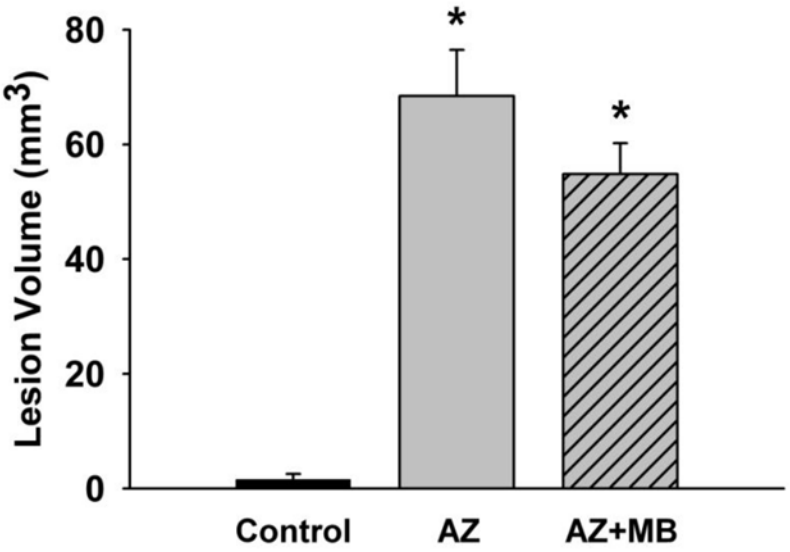

Figure 4. Neuroprotective effects of systemic MB against sodium azide-induced neurotoxicity in the PCC

Quantitative group data for the unbiased stereological analysis of the metabolic lesion volume produced by AZ injections into the PCC. The sham operated control group had less than 2 mm^3 of PCC volume affected. The AZ group showed a PCC lesion volume of about 70 mm^3, whereas the AZ+MB group had a reduced lesion volume averaging 55 mm^3. Therefore, MB treatment induced a total 20% bilateral decrease in the volume of PCC and contiguous cortex affected by structural damage due to cytochrome oxidase inhibition induced by the local infusion of sodium azide. * = significantly different from control, $p < 0.001$.

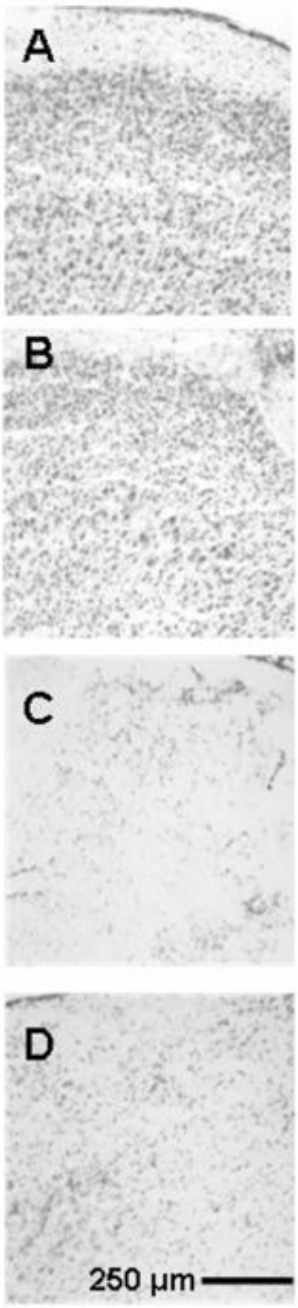

Figure 5. Systemic MB did not prevent the reduction in neuronal density produced by AZ in the dorsal PCC

Representative photomicrographs of high magnification Nissl-stained sections used to count cells at the AZ injection sites in the dorsal PCC to illustrate primary cell counting data. The maximal AZ effect was in the dorsal PCC targeted by the injections, and systemic MB did not prevent neuronal loss in this region. A) Control brain. Section from a sham operated rat not receiving any injections into the PCC, illustrating normal cell density. B) Control vehicle-injected brain. Section from a sham operated rat receiving bilateral vehicle injections into the PCC, illustrating minimal effects on the cell density. C) AZ injected brain. Section from an operated rat that received bilateral AZ injections into the PCC,

illustrating discoloration and neuronal loss in the dorsal PCC. D) AZ+MB injected brain. Section from an operated rat that received bilateral AZ injections into the PCC plus systemic MB, illustrating AZ effects on neuronal density in the PCC that were not statistically different from the AZ group.

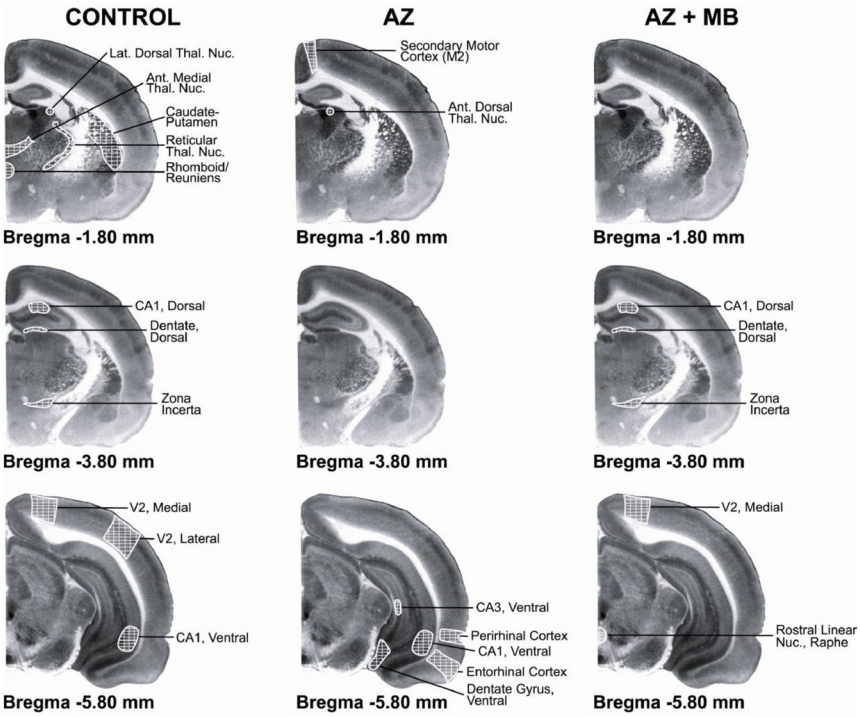

Figure 6. Systemic MB partially prevented the disruption in PCC functional network induced by AZ

Coronal brain sections stained with the cytochrome oxidase histochemistry technique depict the number and anatomical distribution of brain regions showing functional networks with the posterior cingulate cortex (PCC) (white cross-hatching). In control conditions, the metabolic capacity of the PCC was significantly correlated with that of thalamic, hippocampal and extrastriate regions. Except for the ventral CA1, AZ induced a complete loss of this pattern of PCC functional networks, and strengthened PCC connectivity with a different set of hippocampal and parahippocampal regions, as well as with the secondary motor cortex. In contrast, MB not only prevented this new pattern of PCC connectivity, but also partially preserved the PCC connectivity with the hippocampus and the extrastriate cortex as seen in the control. MB also induced coupling between the PCC and the raphe nuclei.

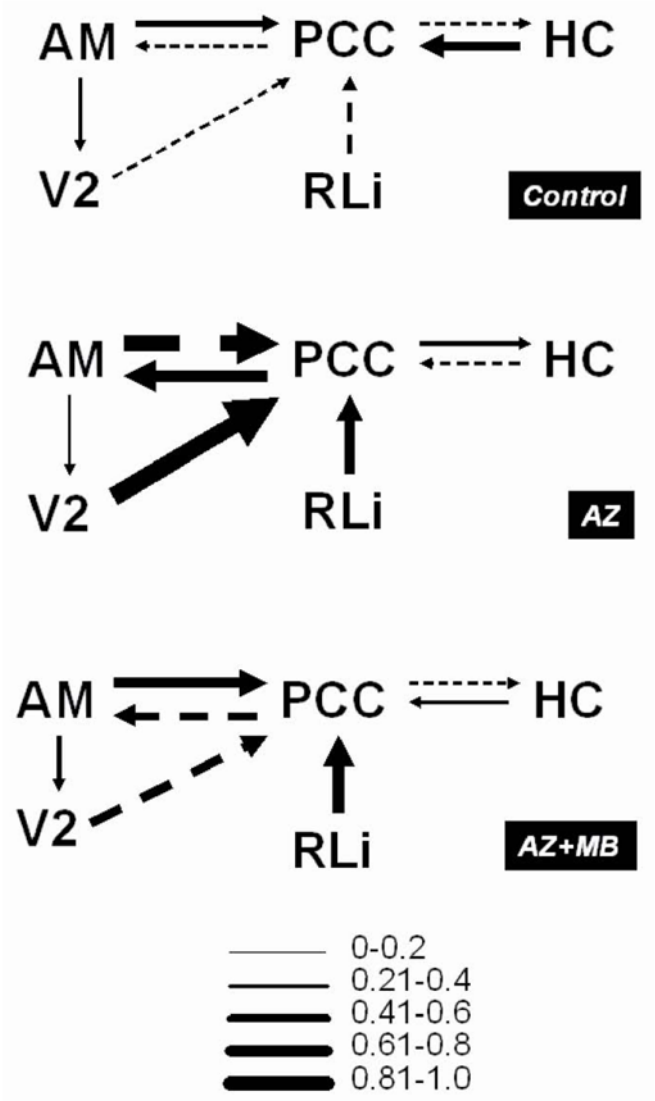

Figure 7. Systemic MB prevented the disruption in PCC effective connectivity induced by sodium azide

Metabolic mapping data was used to construct structural equation models of thalamo-cingulo-hipocampal effective connectivity and determine significant group differences in logical topology. The diagrams represent regions holding direct or indirect anatomical connections (lines). The direction of information flow (effectiveness) is represented by arrowheads and the strength of the effective connection is represented by arrow thickness, which is at the same time, a representation of beta (path) coefficients. Solid lines represent positive and dashed lines negative path coefficients. The control model showed the posterior cingulate/retrosplenial cortex (PCC) having reciprocal connections with the anteromedial thalamic nucleus (AM) and the hippocampus (HC), and receiving negative influences from the secondary visual cortex (V2) and the raphe nuclei (RLi). Azide (AZ) changed the coefficient sign of all PCC inputs and outputs and strengthened the interactions with AM, V2 and RLi. Methylene blue (MB) prevented the changes in PCC effective connectivity, although the strong thalamo-cingular connectivity and the strong recruitment of visual and subcortical regions induced by sodium azide were also observed in the AZ+MB-treated group.

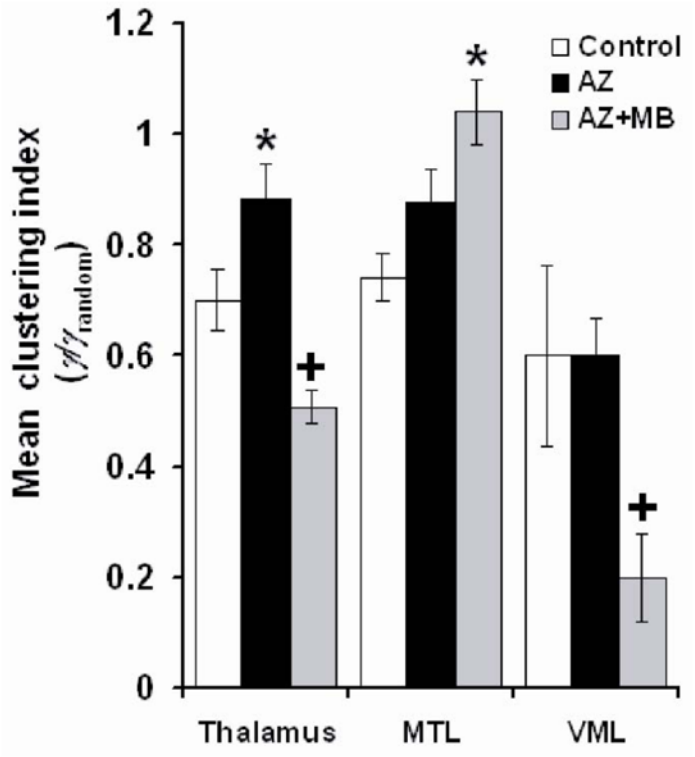

Figure 8. Systemic MB differentially modified the intrinsic connectivity of thalamic, medial temporal lobe, and motor loop networks

Graph theory methods showed that azide (AZ) in the PCC induced an increase in the mean clustering index (γ) (i.e. how close are neighboring regions to be completely interconnected) in the thalamus, but no significant change in that of the medial temporal lobe (MTL) or the visuomotor loop (VML). In each one of the three networks, methylene blue (MB) induced significant γ changes not only compared to AZ but also to control. MB decreased the mean clustering index in thalamic and VML regions, but increased it in the MTL. This differential effect is consistent with the induction of a local activity-dependent adaptive reconfiguration by MB, as opposed to a general and non-specific metabolic-enhancing effect. * = significantly higher than control. + = significantly lower than control, $p < .05$.

Table 1

Locomotor activity in the open field chamber before (Pre) and after (Post) drug treatment

	Control		AZ		AZ+MB	
Measure	**Pre**	**Post**	**Pre**	**Post**	**Pre**	**Post**
Ambulatory time (sec)	35 ± 3	32 ± 3	41 ± 2	43 ± 4	36 ± 2	32 ± 4
Short movement time(sec)	82 ± 3	71 ± 3	79 ± 2	68 ± 3	83 ± 2	72 ± 2
Vertical counts	58 ± 4	49 ± 4	55 ± 3	55 ± 3	50 ± 3	49 ± 5

Table 2

Effects of sodium azide and methylene blue on regional cytochrome oxidase activity

AREA OF INTEREST			CONTROL	AZ	AZ + MB
	abbreviation	**Bregma level (mm)**	**Mean ± SEM *(n)***	**Mean ± SEM *(n)***	**Mean ± SEM *(n)***
CINGULATE REGIONS					
posterior cingulate	PCC	−1.80 to −5.30	299 ± 7 *(10)*	249 ± 11 *(10)* *	215 ± 14 *(9)* *
dorsal PCC	RSA	−1.80 to −5.30	285 ± 8 *(10)*	208 ± 14 *(10)* *	188 ± 15 *(9)* *
ventral PCC	RSG	−1.80 to −5.30	313 ± 6 *(10)*	284 ± 8 *(10)*	242 ± 15 *(9)* *
anterior cingulate	ACC	1.60 to −1.40	304 ± 5 *(10)*	297 ± 4 *(10)*	292 ± 5 *(9)*
cingulum bundle	cb	−1.80 to −5.30	6 ± 5 *(10)*	−6 ± 4 *(10)*	−6 ± 3 *(9)*
THALAMIC REGIONS					
anterior dorsal	AD	−1.80	555 ± 35 *(10)*	542 ± 45 *(10)*	540 ± 30 *(9)*
anterior ventral	AV	−1.80	343 ± 20 *(10)*	362 ± 21 *(9)*	335 ± 25 *(9)*
anterior medial	AM	−1.80	239 ± 7 *(9)*	244 ± 10 *(9)*	234 ± 7 *(9)*
reticular	Rt	−1.80	249 ± 7 *(10)*	267 ± 7 *(10)*	258 ± 7 *(9)*
rhomboid/reuniens	Rh/Re	−1.80	240 ± 7 *(10)*	259 ± 8 *(10)*	244 ± 9 *(9)*
lateral dorsal	LD	−2.30	319 ± 8 *(10)*	325 ± 11 *(10)*	315 ± 5 *(9)*
HIPPOCAMPAL FORMATION					
anterior/dorsal					
CA1	CA1d	−3.80	243 ± 6 *(10)*	244 ± 9 *(10)*	231 ± 8 *(9)*
CA3	CA3d	−3.80	241 ± 7 *(10)*	246 ± 6 *(10)*	242 ± 8 *(9)*
dentate gyrus	DGd	−3.80	323 ± 8 *(10)*	327 ± 4 *(10)*	321 ± 3 *(9)*
posterior/ventral					
CA1	CA1v	−5.30	198 ± 10 *(10)*	210 ± 7 *(10)*	215 ± 9 *(9)*
CA3	CA3v	−5.30	238 ± 8 *(9)*	248 ± 7 *(10)*	251 ± 8 *(9)*
dentate gyrus	DGv	−5.30	192 ± 7 *(10)*	202 ± 7 *(10)*	210 ± 7 *(9)*
subiculum	SUB	−5.30	188 ± 11 *(10)*	197 ± 9 *(10)*	189 ± 13 *(9)*
mammillary bodies	MB	−4.80	296 ± 11 *(7)*	296 ± 8 *(8)*	316 ± 18 *(7)*
entorhinal	Ent	−4.80	165 ± 8 *(9)*	179 ± 8 *(10)*	179 ± 7 *(9)*

AREA OF INTEREST			CONTROL	AZ	AZ + MB
	abbreviation	**Bregma level (mm)**	**Mean ± SEM *(n)***	**Mean ± SEM *(n)***	**Mean ± SEM *(n)***
perirhinal	PRh	−4.80	170 ± 8 *(10)*	183 ± 6 *(10)*	188 ± 9 *(9)*
OTHER					
secondary motor cortex secondary visual cortex	M2	−0.26	268 ± 6 *(10)*	258 ± 2 *(10)*	270 ± 8 *(9)*
medial area	V2M	−5.30	251 ± 13 *(10)*	207 ± 12 *(8)*	240 ± 11 *(9)*
lateral area	V2L	−5.30	249 ± 14 *(10)*	244 ± 10 *(9)*	261 ± 10 *(9)*
caudate putamen	CPu	−1.80	209 ± 8 *(10)*	198 ± 9 *(10)*	215 ± 9 *(9)*
zona incerta	ZI	−3.80	283 ± 8 *(10)*	293 ± 7 *(10)*	269 ± 8 *(9)*
periaqueductal gray	PAG	−5.30	224 ± 8 *(9)*	231 ± 7 *(10)*	223 ± 5 *(9)*
raphe nuclei	RLi	−5.30	168 ± 8 *(6)*	172 ± 15 *(9)*	130 ± 24 *(7)*

* signficantly different from control ($p < .01$)

Table 3

Effects of sodium azide and methylene blue on the functional connectivity of the PCC

Region	Control	AZ	AZ+MB
AD	−.32	.71*	−.21
AM	.67*	.19	.45
Rt	.72*	−.13	−.001
Rh/Re	.68*	.24	.46
LD	.91*	.58	.18
dgd	.75*	.10	.70*
CA1d	.64*	.25	.77*
ZI	.81*	.13	.85*
PRh	.37	.79*	.07
Ent	.30	.93*	.29
DGv	.38	.67*	.17
CA1v	.78*	.65*	.44
CA3v	.33	.79*	.26
RLi	.08	.16	.78*
V2m	.83*	.53	.88*
V2l	.87*	.61	.55
ACC	.76*	.46	.45
M2	.56	.68*	.01
CPu	.66*	.54	.14

d = dorsal, v = ventral, m = medial, l = lateral. See text for abbreviations of regions. Values represent the Pearson product-moment correlations between cytochrome oxidase activity in the PCC and the other brain regions.

*Significantly different from zero ($p < .05$)

Table 4

Connectivity density (κ_{den}) of neural sub-networks after sodium azide and methylene blue

Network	Control	AZ	AZ+MB
Thalamus	0.32	0.39	0.21*
MTL	0.30	0.36	0.53
VML	0.30	0.30	0.10*

MTL = medial temporal lobe, VML = visuomotor loop

*significantly different from random, Z score ± 2.0 ($p < .05$)